Two-Step Method for Instability Damage Detection in Tower Body of Transmission Structures

Weilian Qu[1,*], Wanjun Song[1], Yong Xia[2], Youlin Xu[2], Wenke Qin[1] and Zhicai Jiang[1]

[1]Hubei Key Laboratory of Roadway Bridge and Structure Engineering, Wuhan University of Technology, Wuhan 430070, China
[2]Department of Civil and Structural Engineering, The Hong Kong Polytechnic University, Hung Hom, Kowloon, Hong Kong, China

Abstract: Instability damage may occur in some members of the transmission tower subjected to the downburst, and eventually the damage accumulation may further lead to the failure of the tower. Therefore, it is extremely essential to identify and repair the damaged major vertical members in tower body timely. The relationship surface of instable member among axial compression force, bending moment at the end and axial stiffness is determined. The results show that the axial stiffness of the instability members reduces to zero gradually. Accordingly, a two-step detection method of the major vertical member instability damage is presented. The first step detection is used to find the possible buckling damaged regions by using wavelet packet energy curvature change rate index. The second step is used to identify location of buckling damaged major member that appears in the possible damaged subregions based on the theory of modal strain energy and interval estimation. Finally, the proposed method is applied to a realistic transmission tower and experimental verified with a steel tube tower. The results indicate that the two-step detection method is effective and feasible.

Key words: axial stiffness, damage detection, changing rate of wavelet packet energy curvature, modal strain energy, interval estimation.

1. INTRODUCTION

As a kind of common engineering structure, although there are many researches and practices for engineering design of transmission towers all over the world, wind-induced collapse failures of transmission tower are still reported. According to the disaster investigation in the United States, Australia and South Africa, downburst is one of the main factors leading to the collapse of transmission towers. The reason is that damage may occur in some members of the tower subjected to the downburst, and eventually the damage accumulation may further lead to the failure of the tower. Therefore, many damage detection methods are proposed to prevent transmission tower from collapse.

Albermani (1992 and 2002) predicted the collapse of the transmission tower by adopting nonlinear techniques, and the proposed method was verified by a new tower. Law *et al*. (2011) proposed two kinds of substructure damage detection methods, which detected external excitation and damaged member location in the substructure by time domain signal. Numerical simulation of a simplified model of a transmission tower proved that both methods are effective. Yin *et al*. (2009, 2011) studied damage detection by using ambient vibration signal, which is verified in a full-scale model. Chen *et al*. (2010) detected damage position of the tower by identifying the degradation of structural stiffness by using time domain method, and the proposed method had been applied to an actual tower. Zhu (2009) evaluated damage status of the tower based on neural network analytical method, which was verified to be damage sensitivity by applying to a 500 kV

*Corresponding author. Email address: qwlian1946@163.com; Fax: +86-27-87160361; Tel: +86-27-87160361.

transmission tower. According to the damage property of bolt loose at flange joint of the tower, Tan and Qu (2011) studied damage detection based on wavelet packet feature extraction and fuzzy clustering, which is also experimentally verified in a three-story simplified model of a tower.

Lazarevic *et al*. (2003) partitioned a self-stand transmission tower into several substructures by using hierarchical clustering algorithm, and adopted a two-level neural network to predict the damaged members position according to the variation of measured natural frequencies of the structure on the premise that the relationship between the damaged members location and change of first several natural frequencies of the tower had been established. After transforming the measured acceleration time history signal of the nodal floors of the tower from the time domain to the space domain, Lou *et al*. (2006) applied the space domain wavelet analysis of the statistical moments of the acceleration records to detect the stiffness abrupt change in the vertical direction caused by the structural elements damage, and hence the floor where the damaged members located can be pointed out. However, the presented methods can only be applied to the structures with the well-distributed stiffness along the vertical direction as well as lots of damaged members concentrating a single floor. Qu *et al*. (2007) derived the relationship between the variation of the element stiffness and the nodal displacement of the guyed mast with large slenderness ratio and flexibility, and presented a index to accurate determine the location of damaged vertical elements based on the horizontal time history response. Lin and Xu (2009) detected the damaged major members in a 500 kV transmission tower by combining the neural network theory with frequency change parameters, and results showed that the approach can find the substructure where the damaged elements belong to and both position and extent of the damaged members are also satisfied identified.

The buckling of compression elements of the tower is one of the main reasons that cause the collapse of the transmission tower-line system. However, to the authors' knowledge, few researches focus on the damage diagnosis of compression member instability. As we know, the oblique web member of the tower has large slenderness ratio, so when the applied force exceeds the critical buckling load, it should experience the elasticity instability, which causes the member to lose its bearing capacity suddenly. While as for major member with moderate slenderness ratio, its buckling behavior belongs to elastoplastic instability of compression-bending member. After reaching critical buckling load, the axial stiffness of the member reduces gradually, so the member still can resist some external load. Numerical simulation of the transmission tower subjected to the downburst demonstrates that the instability phenomena may occur in sequence in several inclined web members and major members of the tower. After some major members lose their stability, whether the tower collapses or not mainly depends on the successive downburst time history. Because the inclined web member has little influence on the global stiffness of the tower, the buckling damage identification of the major compression member is of importance for both research and engineering application.

Two-step detection method to diagnose the buckling damage of the transmission tower is presented in the paper. After establishing the relationship between the inner force at the end of the buckling damaged member and axial stiffness, the damage index is determined to descript major member instability. Then, the first step detection is used to find the possible buckling damage region according to the change rate of wavelet packet transform (WPT) energy curvature of acceleration response of every nodal floor of the tower. The second step is used to specify the position of buckling damaged members based on the difference between the modal strain energy change rate of every major member at potential damaged region and upper limit of confidence interval in probability statistical. Both numerical simulation and experimental result illustrate that the proposed method can effectively judge buckling damaged region of the tower as well as detect accurately location of the buckling damaged members.

2. THEORY AND METHOD

2.1. Buckling Damaged Index of Major Member for Tower Body

Time history response of the transmission tower subjected to the downburst shows that, before collapse of the tower, inclined web members first lose their stability and then buckling occurs in major members. After some major members lose their stability, some towers may collapse totally, while some other towers still can stand, which mainly depends on the successive downburst time history. Since oblique web member has potty effect on the global stiffness of the tower, the influence of buckling damaged web member on tower collapse is negligible. Therefore, timely monitoring of the instability damage status of major member is very crucial to improve the damaged tower

safety because buckling compression members can be repaired in time.

According to the buckling experiment, as for the compression-bending member with moderate slenderness ratio, the relationship between the axial inner force at the end of the element and the axial stiffness before and after buckling can be shown in Figure 1. It can be seen that the element axial stiffness reduces gradually and the member can still bear some external load after elastoplastic buckling occurs. Consequently, axial stiffness of the major member of the tower can be selected as a reasonable buckling damaged index.

Although there are some other factors to mitigate axial stiffness of the member, these factors almost impossibly occur in the transmission tower according to the in-site investigation. Noted that before major member buckling occurs, at least one web member of the tower definitely loses its stability. The web member instability belongs to elastic buckling, which causes the web member axial stiffness to be null. Therefore, in the strict sense, when the axial stiffness reduction of major members is detected as well as the zero stiffness is identified in some web members simultaneously, it should be convinced that the major bar is undergoing buckling damage. Thus the stiffness reduction of the major member can be considered as a symbol of buckling

2.2. Identification Method of Possible Buckling Damaged Subregion of Tower Body

The first step detection is used to find the possible buckling damaged regions of the transmission tower. Accelerometers (Figure 2) are installed at every nodal floor of the tower to measure the acceleration response caused by wind load, from which the change status of the WPT energy curvature distributed along the tower height can be obtained.

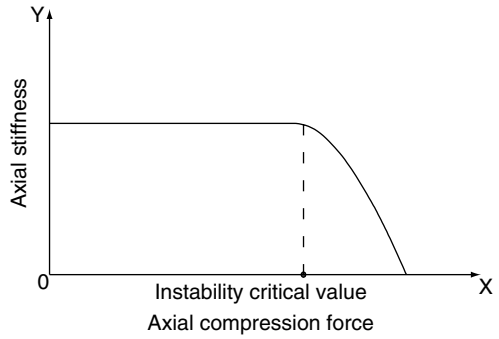

Figure 1. Relationship between axial compression force and axial stiffness of element with constant bending moment at end

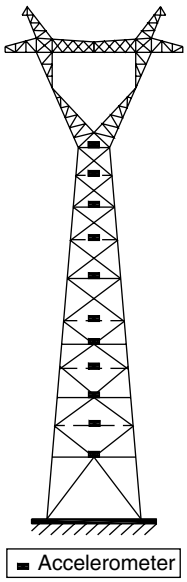

Figure 2. Layout of installed accelerometers

The tower is first partitioned several subregions according to nodal floor. If the major members in a subregion lose their stability, then the dynamic characteristics of the exact nodal floor with damaged members and the adjacent nodal floors will alter compared with the original tower. Therefore the acceleration response of every nodal floor for the original and damaged tower is decomposed and reconstructed by WPT to obtain energy distribution variation in each freqeuncy band, and correspondingly the possible subregion where the buckling damaged member locates can be detected (Yen and Lin 2000; Sun *et al*. 2005; Law *et al*. 2005). The detailed steps are listed as follows (Chang and Sun 2005):

1) To decompose the acceleration signal of nodal floor of the tower into *j*th levels by using WPT to obtain the total 2^j frequency bands with equal width and then to extract signal decomposition coefficients $X_j^i (i = 1, 2...2^j)$ from low to high frequency in sequence, which are reconstructed to obtain signal $f_j^i(t)$ in every frequency band range.
2) To calculate the WPT energy in every frequency band range. Let E_j^i is signal energy at *i*th nodal floor at *j*th level resolution, which is defined as

$$E_j^i = \int_{-\infty}^{+\infty} \left| f_j^i(t) \right|^2 dt \tag{1}$$

After all E_j^i are calculated, WPT energy distribution at each nodal floor of the tower is known.

3) To define the WPT energy curvature of the *i*th frequency band at the *k*th nodal floor as

$$EC^i_{j,k} = \frac{2l_{(k-1),k}\left(E^i_{j,(k+1)} - E^i_{j,k}\right) - 2l_{k,(k+1)}\left(E^i_{j,k} - E^i_{j,(k-1)}\right)}{l_{(k-1),k}\cdot l_{k,(k+1)}\cdot l_{(k-1),(k+1)}} \tag{2}$$

In which $E^i_{j,(k-1)}$, $E^i_{j,k}$ and $E^i_{j,(k+1)}$ are WPT energy at the $(k-1)$th, kth and $(k+1)$th nodal floor, respectively. $l_{(k-1),k}$ is the distance between the $(k-1)$th and kth nodal floor, and the meanings of $l_{k,(k+1),k}$ and $l_{(k-1),(k+1)}$ can be deduced by analogy.

4) To define the change ratio of WPT energy curvature of the *i*th frequency band at the *k*th nodal floor as

$$ECCR^i_{j,k} = \left|\frac{EC^{i,d}_{j,k} - EC^{i,u}_{j,k}}{EC^{i,u}_{j,k}}\right| \tag{3}$$

In which, superscript *u* and *d* stands for the original undamaged and damaged tower, respectively. Accroding to the change ratio of WPT energy curvature of the *i*th frequency band at every nodal floor, the possible region which contains buckling damaged members can be identified.

2.3. Location Identification of Buckling Damaged Major Member for Possible Buckling Damaged Subregion

The second step of the proposed method in the paper is used to identify location of buckling damaged major member of the tower. Speedometers (Figure 3) are installed at every node to measure the wind-induced velocity response. After measuring the velocity response of the tower, the displacement result can be calculated by simple integral operation. Then the change ratio of modal strain energy of all members, which includes both damaged bars and undamaged ones, can be obtained. Furthermore, the upper limit of change ratio with a certain confidence probability is also derived.

The buckling damaged major member of the tower mostly can be described as the axial stiffness reduction of the element, which will induce the change of structural modal parameters, such as modal shape and natural frequency. Therefore, the modal strain energy of the element, which is a function of element stiffness and modal shape, also changes

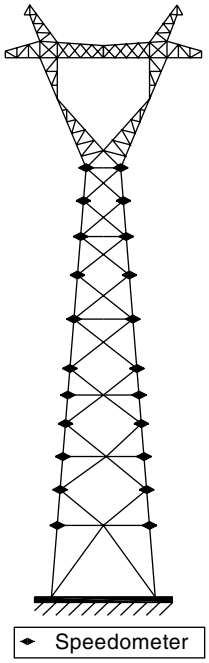

Figure 3. Layout of installed speedometers

(Devore and Jay 2000; Shi *et al*. 1998; Yan *et al*. 2010). As for a cantilever structure, when initial displacement symmetrically applied at the top of the structure, the free vibration is dominated by the first order lateral-bending mode (the first order torsional mode should be included additionally if only one major member is buckling).

1) The *i*th modal strain energy of the *j*th element is defined as

$$MSE^i_j = \{\phi_i\}^T [K_j] \{\phi_i\} \tag{4}$$

where $\{\phi_j\}$ denotes the *i*th modal shape; $[K_j]$ denotes the element stiffness matrix of the *j*th element.

2) After higher order terms are omitted, the variation of modal strain energy MSE^i_j before and after buckling damage occurring is

$$MSEC^i_j = MSE^{i,d}_j - MSE^{i,u}_j = 2\{\phi_i\}[K_j]\{\Delta\phi_i\} \tag{5}$$

in which the superscript *d* means the damaged tower.

3) According to Reference (Shi *et al*. 1998), the variation of the modal strain energy of the damaged element is significant, while that of the adjacent undamaged member is small, and that of the member, which is far away from the damaged one, is tiny. This hints that the modal

strain energy change ratio (*MSECR*) can serve as locating index to denote buckling damaged member. The *MSECR* of the *i*th mode at the *j*th element is defined as

$$MSECR_j^i = \left| \frac{MSE_j^{i,d} - MSE_j^{i,u}}{MSE_j^{i,u}} \right| \tag{6}$$

In order to overcome the random noise influence on experimental mode shapes, multi order mode shapes are measured and the $MSECR_j$ of the *j*th element is defined as the average of the summation of $MSECR^i_j$ of all the modes normalized with respect to the largest value $MSECR^i_{\max}$ of each mode.

$$MSECR_j = \frac{1}{m} \sum_{i=1}^{m} \frac{MSECR_j^i}{MSRCR_{\max}^i} \tag{7}$$

4) As mentioned in the above section, the subregions which contain damaged major members have been detected at first by WPT energy curvature change ratio, so the scope of damaged region reduces effectively. In these subregions the variation of modal strain energy of the damaged member is dramatic, while that of the other bar is neglectable. The *MSECR* of the *i*th mode at every member in the region is taken as a sample. The one member, whose MSECR is larger than the upper confidence limit of the mean value of the sample, is considered as buckling damaged member.

Assuming the MSECR of the *i*th mode at an element to be a random variable with normal distribution, that is,

$$MSECR_j \sim N(\upsilon, \sigma^2), j = 1,2,\cdots,ne \tag{8}$$

in which *ne* is sum of elements in the possible damaged subregion. The calculated MSECR of the *i*th mode at every member in the subregion is taken as a realization of the random variable. Then the mean value and standard deviation of these realizations are $\bar{x}$ and *s*, respectively. The T-distribution is obtained as

$$\frac{\overline{X} - \upsilon}{S / \sqrt{ne}} \sim t(n-1) \tag{9}$$

The upper limit of mean value μ with confidence probability $1 - \alpha$ is given by

$$\mu = \overline{X} + \frac{S}{\sqrt{ne}} t_{\frac{\alpha}{2}}(n-1) \tag{10}$$

Then the damage locating index of the *j*th member is selceted as

$$Index_j = MSECR_j - \mu \tag{11}$$

If $Index_j \geq 0$, the *j*th member has damage at the confidence level $1 - \alpha$, otherwise the member is considered as undamaged.

3. CASE STUDY

3.1. Structural Information

An actual transmission tower (Chen *et al*. 2009) is taken as a numerical example to investigate the feasibility of the proposed damage detection approach. The total height of the transmission tower is 105.8 m, and the tower body is 78.0 m high. The simplified model of the tower is illustrated in Figure 4. The tower body is divided into 11 nodal layers and 10 subregions as shown in the Figure 4. The major vertical members can be classified into two types, whose physical parameters are listed in Table 1.

3.2. Relationship between Axial Compression Force, Bending Moment and Axial Stiffness of Elastoplastic Instability Major Vertical Member

The major vertical members may experience instability under the axial compression force. The instability of steel members is substantially controlled by the element stiffness (Sun *et al*. 2005). The elastoplastic

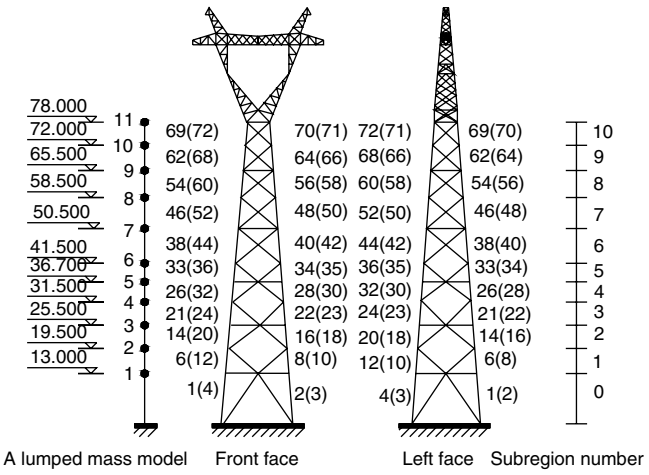

Figure 4. Simplified model of the tower

Table 1. Physical parameters of the major vertical members

Member type	I	II
Outer radius (m)	0.15	0.15
Inner radius (m)	0.11	0.13
Young's modulus E(N/m$^{2)}$	2.06×10^{11}	2.06×10^{11}
Mass density ρ(kg/m^3)	7850	7850
Location	from subregion 0 to 5	from subregion 6 to 10

instability characteristics can be investigated by examining the axial stiffness reduction of the major members in this study. The finite element model of major vertical members is constructed by using commercial finite element analysis package ANSYS.

Figure 5(a) shows the fine finite element model of a typical major member, which is modeled by a Solid45 element. The Poisson's ratio of steel material is 0.3. A constant bending moment is applied on the member ends and the applied axial compression force increases gradually to analyze the member buckling with arc-length method. When the fix-end axial force and relative axial displacement are obtained, the axial stiffness is obtained by the first derivative of axial force with respect to axial displacement, which is calculated practically by finite difference method. The elastoplastic instability process is shown in Figure 5. The bending deformation development of major member is amplified by ten times for clear observation.

Red means the stress of the member is in the elastic range, and gray means the element stress exceeds yield strength entering into the plastic range in Figure 5. When the axial compression force is small, the stress of the member is in the elastic range and bending deformation is small, as shown in Figure 5(b). With the increase of axial compression force, the member stress and the bending deformation also increase as shown in Figure 5(c). When the axial compression force reaches a certain value, the stress in part region enter into the plastic range and bending deformation further improves, as shown in Figure 5(d). Then the plastic zone in the cross section of the compression member enlarges and the bending deformation further increase, as shown in Figure 5(e). When the axial compression force reaches a certain threshold, the plastic zone in the cross section becomes wider and correspondingly the elastic region resisting axial compression force shrinks significantly. Meanwhile, if the bending deformation is too large, the compression member should lose its stability, as shown in Figure 5(f).

Figure 6 shows the relationship between axial compression, bending moment and axial stiffness. It is seen that with the increase of end bending moment of member, the maximum allowable axial compression force decreases. If the end bending moment is absent, the maximum axial compression force is 6200 kN. If the end bending moment is 620 kN·m, the member can carry axial compression force 1650 kN only. Figure 6 indicates that if the stress of the member is in the elastic range, the axial stiffness remains no change. If the member is in the plastic stage, the axial stiffness gradually decreases with the increasing plastic area. Besides, with the increase of end bending moment, maximum allowable axial force is lowered gradually.

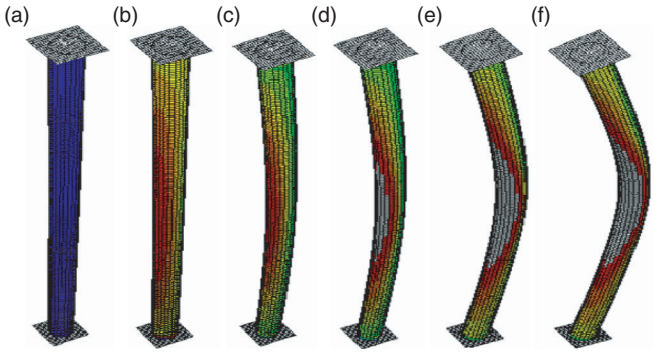

Figure 5. The elastoplastic instability process of the major vertical member

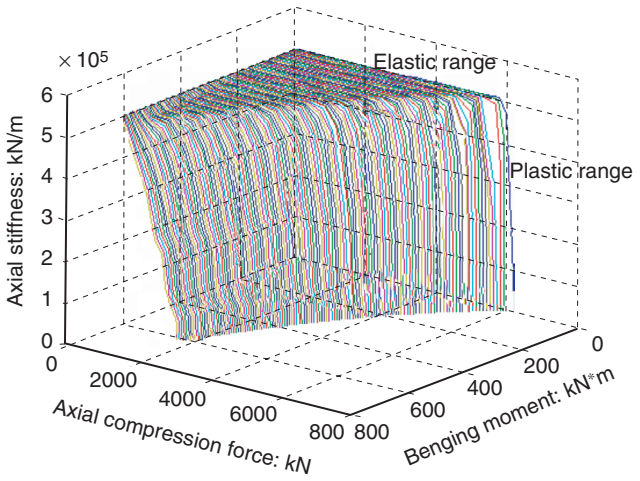

Figure 6. 3D curved face of axial compression force-bending moment-axial stiffness relationship

3.3. Damage Detection

As mentioned above, the instability damage can be simulated by the reduction of the element axial stiffness. Two damage cases listed in Table 2 are investigated. Only the instability damage at the major vertical members is considered in this study. Case 1 is that all the instability damaged members are in one subregion and Case 2 in two subregions.

3.3.1. Detection of possible damaged subregion

A rectangular impulse is applied on the top of tower in the x direction and the first 10 seconds acceleration responses in the x direction at 44 nodes of all 11 nodal layers with/without damage are computed. The response time histories are decomposed into three levels by using bior6.8 wavelet and WPT energy of the first frequency band are calculated. The change rate of energy curvature before and after damage for Cases 1 and 2 are shown in Figure 7 and Figure 8, respectively.

It is seen from Figure 7 that the change rates of energy curvature at the 5th and 6th nodal floors are significant for Case 1. Thus, the instability damage events may exist in Subregions 4, 5, and 6. Figure 8 demonstrates that the change rates at the 3rd, 6th, and 7th nodal floors are remarkable. Therefore, the instability damage may exist in Subregions 2, 3, 5, 6 and 7.

Table 2. Damage cases of the transmission tower

Case	Damaged members	Damage extent	Damaged subregion
1	33	30%	5
	36	40%	5
	24	50%	3
2	38	40%	6
	44	45%	6

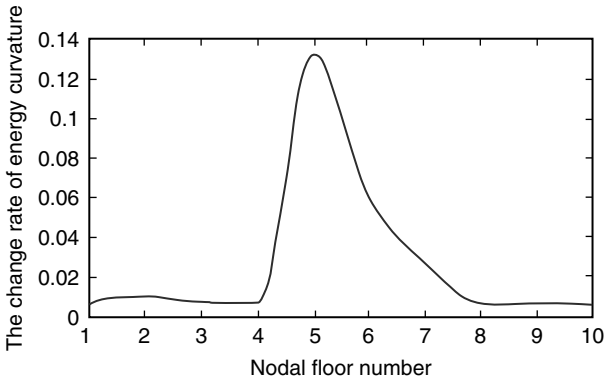

Figure 7. Detection results for Case 1

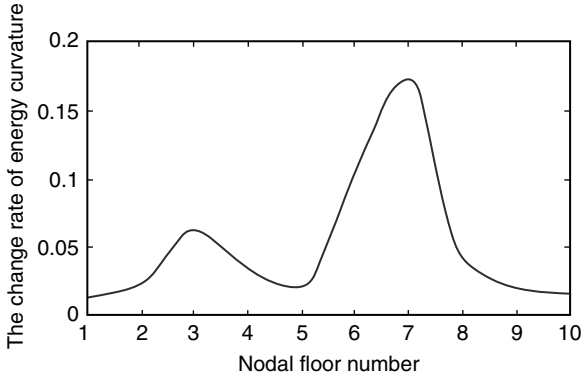

Figure 8. Detection results for Case 2

3.3.2. Detection of damage member location for possible damaged subregion

As for the cantilever structure, when the initial structural vertical displacement distribution is similar with the first order mode shape, it can be approximately considered that the structural free vibration is dominated by the first order mode shape, therefore at the same instant between different nodal layers the relative displacement ratio of dynamic response is assumed to be that of the first order mode shape according to the superposition theory. The modal strain energy of the first two mode shapes of the transmission tower in the two orthogonal directions is calculated. Rotational mode shapes are not involved. From the proposed damage detection approach, the damage indexes of the members in the possible subregions are calculated.

For Case 1, the modal strain energy change rate which is calculated by Eqn 7 of all major vertical members in the Subregions 5, 6 and 7 are listed in Table 3. As mentioned before, $MSECR_j$ is assumed to be random variable obeying normal distribution. From Table 3 the mean value and standard deviation are 0.18521 and 0.30447, respectively. The sum of members in the possible damaged region ne is 12, and the confidence level $1 - \alpha$ is 95%. The damage indexes of members are calculated by Eqn 11 and graphically presented in Figure 9. It demonstrates that only the damage indexes of member 33 and 36 are larger than zero, indicating that the appointed damaged members are accurately detected.

For Case 2, the modal strain energy change rate which is calculated by Eqn 7 of all major vertical members in the Subregions 2, 3, 5, 6 and 7 are listed in

Table 3. Modal strain energy change rate for Case 1 (1% noise)

Member no.	$MSE_j^{1,u}$	$MSE_j^{1,d}$	$MSE_j^{2,u}$	$MSE_j^{2,d}$	$MSECR_j^1$	$MSECR_j^2$	$MSECR_j$
26	0.99961	0.89475	1.247	1.1943	–0.10877	–0.047954	0.05414
28	0.99859	1.0598	1.2482	1.1943	0.043607	–0.022318	0.02309
30	0.99956	0.88722	1.2470	1.3712	–0.11128	0.098049	0.077316
32	0.99855	0.99157	1.2482	1.0194	–0.0041354	–0.18235	0.082862
33	1.8794	3.3121	2.3330	4.3808	0.74216	0.8978	0.62481
34	1.8773	1.9999	2.3354	2.2398	0.077987	–0.040368	0.041497
35	1.8789	1.6496	2.3329	2.5932	–0.11162	0.11049	0.082986
36	1.8769	5.0026	2.3353	4.9856	1.6644	1.1171	1.0000
38	2.4994	2.3055	3.0316	2.9706	–0.07457	–0.017241	0.030119
40	2.4971	2.6218	3.0345	2.8892	0.051757	–0.060607	0.042676
42	2.4990	2.1957	3.0317	3.3422	–0.123	0.11028	0.086315
44	2.4967	2.5868	3.0347	2.5619	0.043599	–0.14209	0.076697

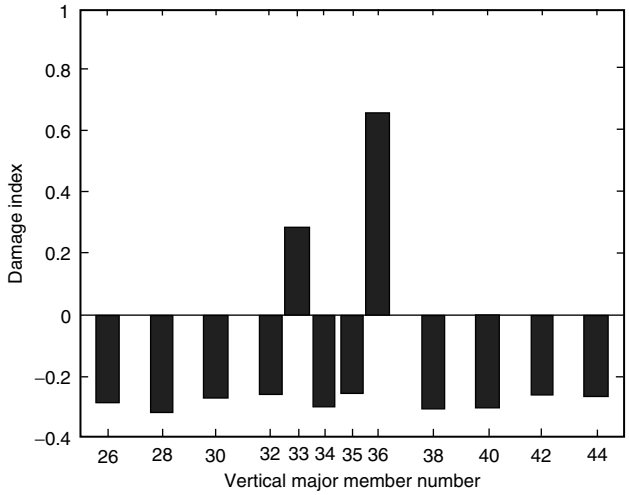

Figure 9. Detection results for Case 1

Table 4. The mean value and standard deviation of $MSECR_j$ are 0.19804 and 0.20880, respectively. The sum of members in the possible damaged region *ne* is 20, and the confidence level $1 - \alpha$ is 95%. The damage indexes of members are calculated by Eqn 11 and graphically presented in Figure 10. The data in Figure 10 indicates that only the damage indexes of members 24, 38 and 44 are larger than zero, again indicating that the preassigned damaged members are accurately detected.

4. EXPERIMENTAL VERIFICATION

4.1. Introduction of the Experiment

A six-floor tower model is shown in Figure 11 and Figure 12. The plan size is 0.5 m × 0.5 m, and total height 4.5 m. The major vertical members are made of seamless circular

Table 4. Modal strain energy change rate for Case 2 (1% noise)

Member no.	$MSE_j^{1,u}$	$MSE_j^{1,d}$	$MSE_j^{2,u}$	$MSE_j^{2,d}$	$MSECR_j^1$	$MSECR_j^2$	$MSECR_j$
14	1.3016	0.91415	1.6525	1.7332	–0.30256	0.040398	0.05945
16	1.3003	1.6184	1.6541	1.2252	0.25527	–0.25539	0.11242
18	1.3014	0.79725	1.6527	2.0761	–0.37971	0.25896	0.1332
20	1.3001	1.3704	1.6543	0.96555	0.037309	–0.4217	0.12457
21	1.4984	1.0289	1.9014	2.0092	–0.32327	0.033786	0.060881
22	1.4968	1.8917	1.9032	1.3888	0.27104	–0.27072	0.11924
23	1.4981	0.90192	1.9015	2.4133	–0.40037	0.25637	0.13576
24	1.4965	6.1622	1.9033	3.9976	3.1461	1.1132	0.8132
33	1.8794	1.3508	2.333	2.4832	–0.2754	0.069792	0.063405
34	1.8773	2.3348	2.3354	1.7604	0.25254	–0.23345	0.10582
35	1.8789	1.0629	2.3329	3.1366	–0.42699	0.35244	0.16702
36	1.8769	2.2048	2.3353	1.2803	0.18258	–0.45529	0.15711
38	2.4994	4.4139	3.0316	8.3873	0.787	1.7772	0.62508
40	2.4971	3.1027	3.0345	2.2976	0.22758	–0.25048	0.10664
42	2.499	1.558	3.0317	4.015	–0.37666	0.32409	0.15104
44	2.4967	8.5114	3.0347	4.9572	2.4037	0.6327	0.56002
46	1.917	1.3755	2.2643	2.416	–0.29401	0.06701	0.065579
48	1.915	2.3381	2.2665	1.7427	0.22408	–0.23352	0.10131
50	1.9168	1.2352	2.2643	3.0126	–0.36239	0.34506	0.15468
52	1.9148	2.1684	2.2664	1.318	0.14846	–0.42936	0.14439

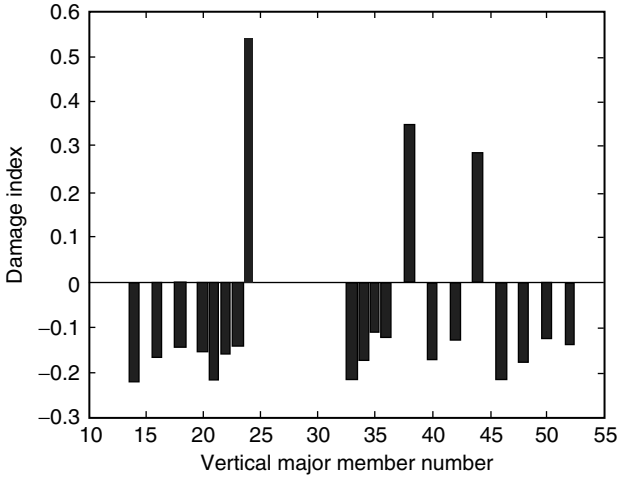

Figure 10. Detection results for Case 2

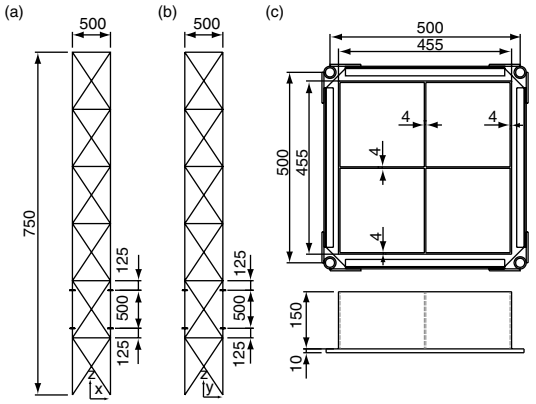

Figure 12. Dimensions of the model: (a) front face; (b) left face; and (c) floor

Figure 11. Tower model

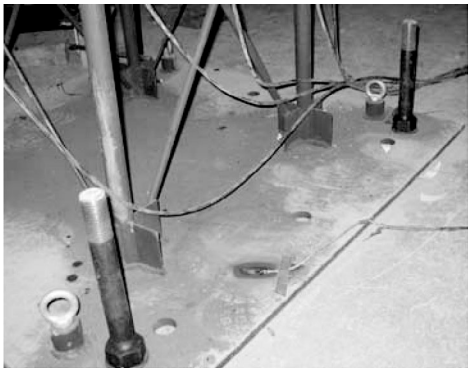

Figure 13. Foundation connection

steel tube with 16 mm external radius and 12 mm inner radius. The braces in *x* direction are made of solid circular steel with 3 mm radius, and the braces in *y* direction are made of solid circular steel with 7 mm radius. The beams are made of angle steel with 25 mm × 4 mm, and each floor is made of steel plate with 10 mm thick. The beams, vertical members, and braces are welded to each other by small steel gusset plates (150 mm × 65 mm × 4 mm), and the floors are welded to the beams. The first four floors have 240 kg additional weight each, and the top two floors have 120 kg additional weight each. At the ground level, each major vertical member is welded to a thick steel plate which is fixed to the ground floor using four bolts, as shown in Figure 13. The size and material parameters of member are summarized in Table 5.

There are two pairs of flanges at both ends of the four major vertical members on the second floor of the tower model. Each pair of flange is fixed by 6 hexagon bolts with 3 *mm* radius. The position and dimensions of the flange are shown in Figure 12(a) and Figure 14, respectively.

In the experiment, five SPC-51 accelerometers made in Japan are located in the four lower floors and the roof to measure the acceleration response. The recording time is 120 *s* and the sampling frequency is 200 Hz. Six DH610 speedometers made in China are located at both ends of vertical member 1, 2 and 3 in Subregion 1, as shown in Figure 15. The recording time is 25 *s* and the sampling frequency is 200 Hz.

4.2. Damage Detection

To validate the efficiency of the proposed two-step detection method, the instability damage in the major

Table 5. Cross-sections size and material properties of different members of the tower model

	Section	Outer radius (m)	Thickness (m)
Major vertical member	Circular tube	1.6×10^{-2}	4.0×10^{-3}
Major vertical member to simulate damage	Circular tube	5.0×10^{-3}	1.0×10^{-3}
Braces in x direction	Solid circular	3.0×10^{-3}	–
Brace in y direction	Solid circular	7.0×10^{-3}	–
Beam	Angle iron	–	4.0×10^{-3}
Floor	Plate	–	1.0×10^{-2}

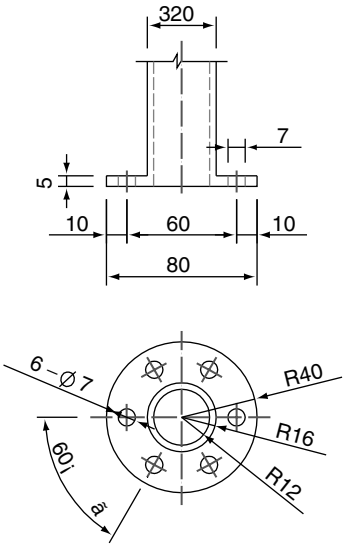

Figure 14. Dimensions of flange

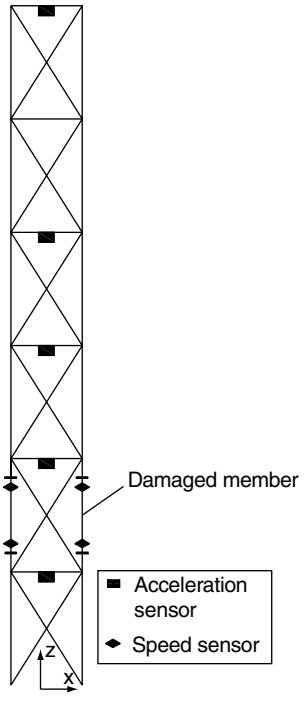

Figure 15. Sensors position

vertical members is simulated in the experimental study, by replacing one major vertical member on the second floor with a bar with smaller cross section. The major vertical member 3 is the "damaged" member. The detailed position and dimension of this "damaged" member are shown in Figure 15 and Table 5, respectively.

4.2.1. Step 1: detection of possible damaged subregion

Only the instability damage of the major vertical members is considered in this study. The tower body is divided into 5 nodal floors and 4 subregions as shown in Figure 16. Free vibration of the structure is generated by releasing it with an initial deflection. The 120 seconds acceleration responses of five nodal floors in the *x* direction with/without damage were measured, as shown in Figure 17 and Figure 18, respectively.

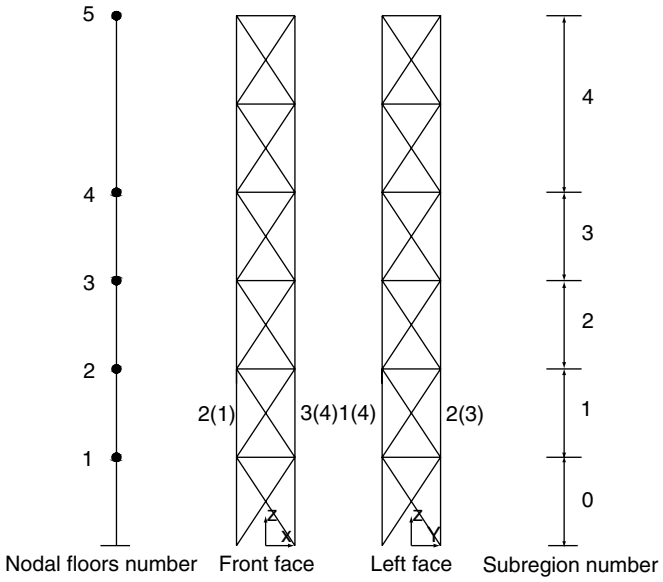

Figure 16. Nodal floor and Subregion numbers of the model

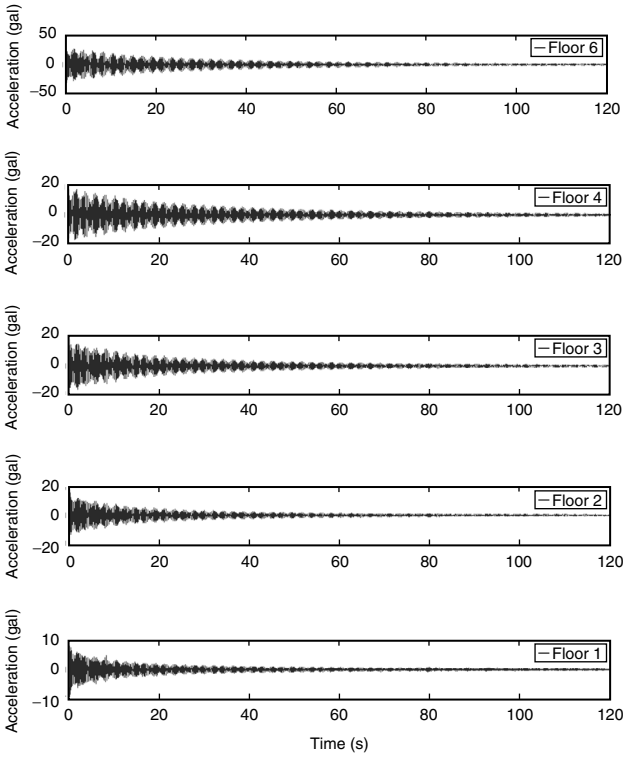

Figure 17. Acceleration responses of 5 nodal floors without damage

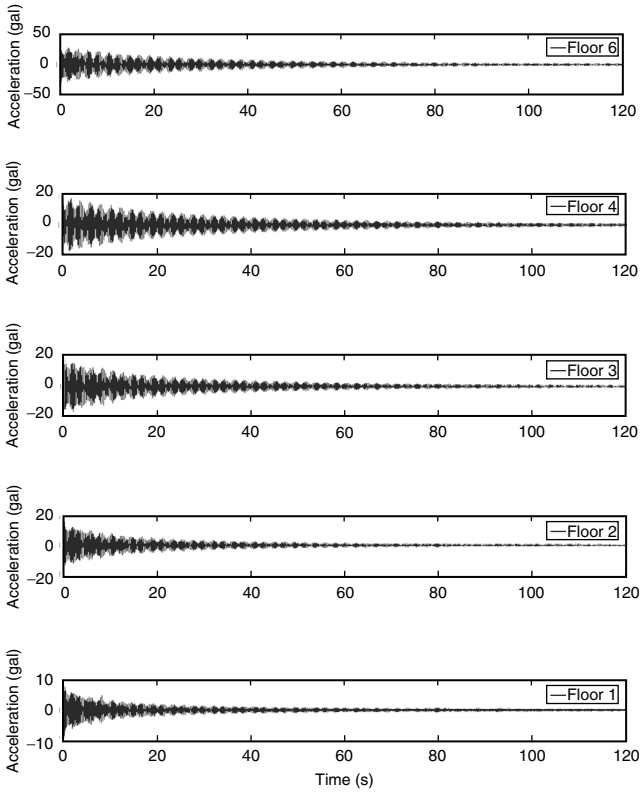

Figure 18. Acceleration responses of 5 nodal floors with damage

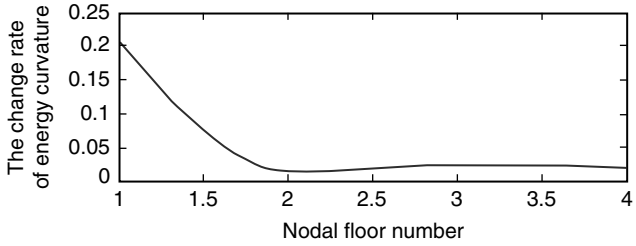

Figure 19. Detection results for possible regions of instability damage of major members

The response time histories are decomposed into three levels using bior6.8 wavelet and the WPT energy of the first frequency band are utilized to construct the change rate of energy curvature. The detection result is shown in Figure 19.

Figure 19 shows that the change rate of energy curvature at the first nodal floor is much larger than others, indicating that the instability damage may exist in Subregion 1.

4.2.2. Step 2: damaged member location for possible damaged subregion

The possible region containing instability damaged member is determined in the previous section. The displacement responses at both ends of major vertical member 1, 2 and 3 in Subregion 1 in x direction with/without damage are calculated by the simple integral of measured velocity signals, as shown in Figure 20 and Figure 21, respectively.

When a major vertical member is damaged, the stiffness distribution of the damaged region will change and cause the alteration of the dynamic characteristic, and the 2nd torsional mode is the dominated one. Figure 22 shows the measured 2nd mode shape components in x direction of the Members 1, 2 and 3 with and without buckling damage. The modal strain energy change rate which is calculated by Eqn 6 of Members 1, 2 and 3 are listed in Table 6. Taking $MSECR_j^2$ as an event set of random variable, the mean value and standard deviation are 0.56368 and 0.35085, respectively. The sum of members in the possible damaged region ne is 3, and the confidence level $1 - \alpha$ is 75%. The damage indexes of member are calculated by Eqn 11 and graphically presented in Figure 23.

Figure 23 demonstrates that only the damage index of Member 3 is larger than zero among the possible damaged three members. This implies that Member 3 is damaged, which is the same as the actual situation.

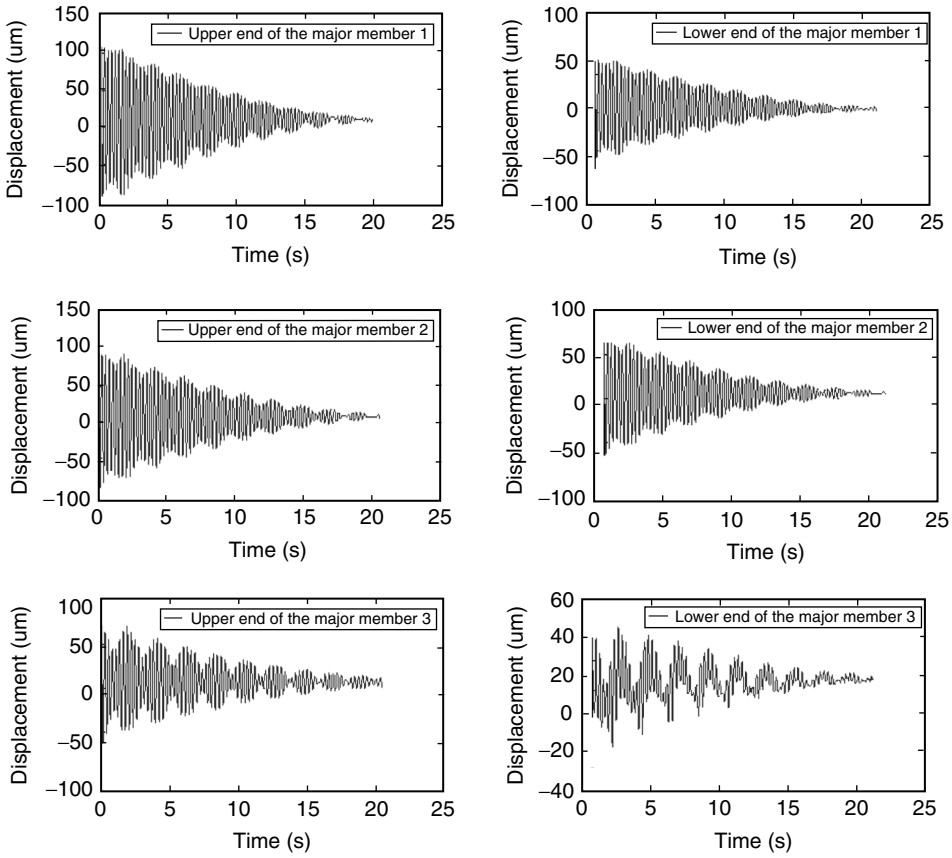

Figure 20. Displacement time histories at the end of three major vertical members in x direction without damage

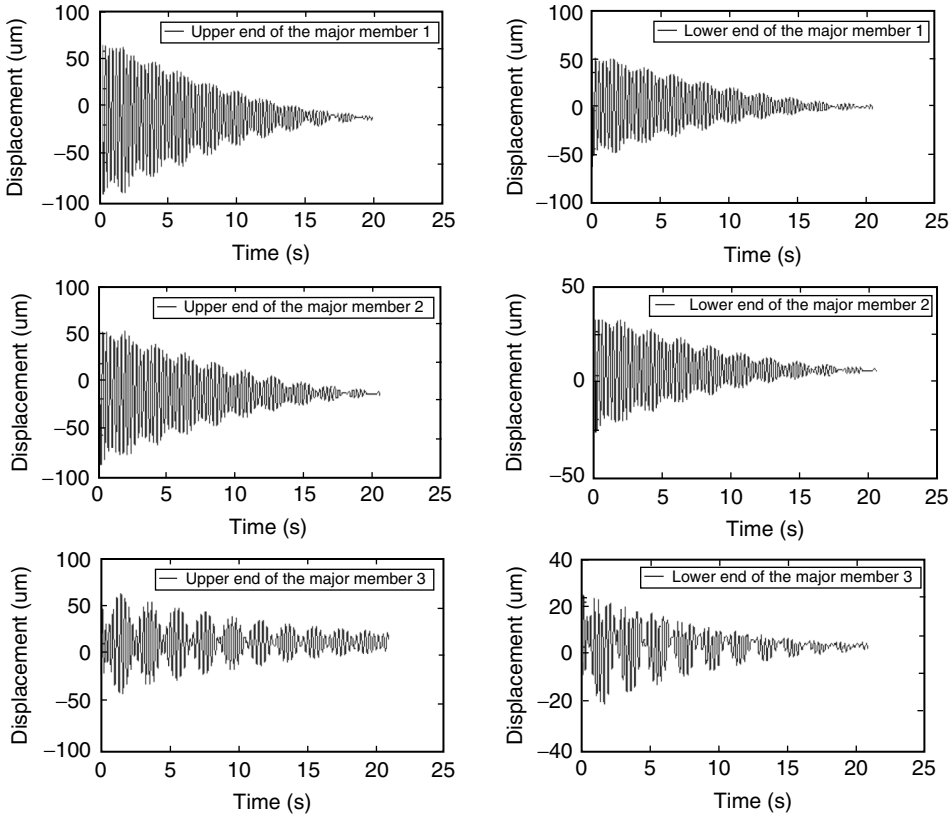

Figure 21. Displacement time histories at the end of three major vertical major members in x direction with damage

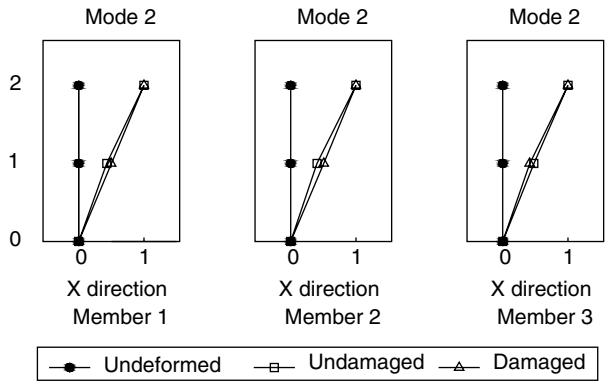

Figure 22. Measured mode components in x direction before and after damage

Table 6. Modal strain energy change rate

Member number	$MSE_j^{2,u}$	$MSE_j^{2,d}$	$MSECR_j^2$
1	39590	28002	0.29270
2	35505	19939	0.43841
3	5380.8	10546	0.95993

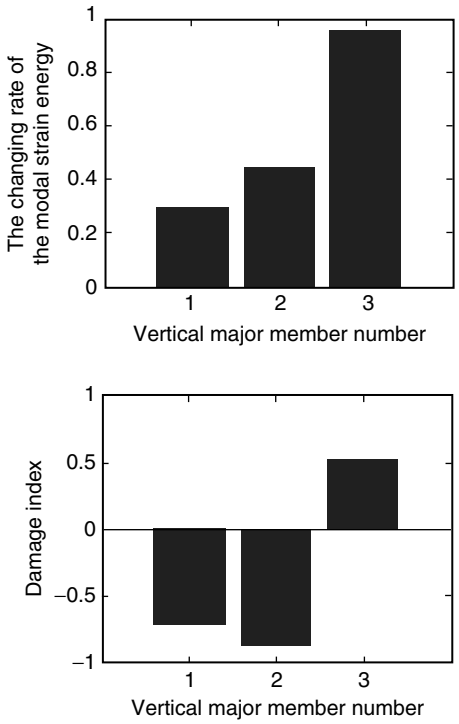

Figure 23. Detection results for damaged member location (confidence level 75%)

5. CONCLUSIONS

A two-step detection method of instability damage of major vertical members in transmission towers is proposed in this study. The relationship among axial compression force, bending moment, and axial stiffness of the major member is established by using the finite element method. Numerical simulation and experimental study indicate that the proposed two-step approach is accurate. Some conclusions can be drawn as follows:

1) The major vertical members of a transmission tower can remain partial load-bearding capacity when subjected to elastic-plastic instability damage. The member axial stiffness may decrease to some extent. If the middle section of the major vertical member is in elastic stage, the axial stiffness does not decrease. If the middle section of the vertical major member is in plastic stage and the axial force is larger than the crucial value, the member axial stiffness gradually decreases to zero.
2) The numerical simulation and experiment carried out in this study indicate that the proposed two-step damage detection method can accurately identify the location of instability damaged major vertical members.
3) The proposed two-step diagnosis method still works if the detection order is reversed, that is, the method used in the second step is firstly applied to identify instability major members in all subregions of tower body, and then these identified members will be verified by approach adopted in the first step.

ACKNOWLEDGEMENTS

The authors wish to acknowledge the financial supports from the National Natural Science Foundation of China (NNSFC-50830203 and NNSFC-50978209).

REFERENCES

Albermani, F. and Kitipornchai, S. (1992). "Nonlinear analysis of transmission towers", *Engineering Structures*, Vol. 14, No. 3, pp. 139–151.

Albermani, F., Kitipornchai, S. and Chan, R.W.K. (2009). "Failure analysis of transmission towers", *Engineering Failure Analysis*, Vol. 16, No. 6, pp. 1922–1928.

Chang, C.C. and Sun, Z. (2005). "Structural damage localization using spatial wavelet packet signature", *Smart Structures and Systems*, Vol. 1, No. 1, pp. 29–46.

Chen, B. Zheng, J. and Qu, W. (2009). "Control of wind-induced response of transmission tower-line system by using magnetorheological dampers", *International Journal of Structural Stability and Dynamics,* Vol. 9, No. 4, pp. 661–685.

Chen, B., Zheng, J. and Qu, W. L. (2010). "Vibration control and damage detection of transmission tower-line system under earthquake by using friction dampers", *Proceedings of the 11th International Symposium on Structural Engineering,* Guangzhou, China, December, pp. 1418–1425.

Devore, J.L. (2000). *Probability and Statistics for Engineering and the Sciences,* 5th Edition, Duxbury, Australia.

Lam, H.F. and Yin, T. (2011). "Dynamic reduction-based structural damage detection of transmission tower: Practical issues and experimental verification", *Engineering Structures*, Vol. 33, No. 5, pp. 1459–1478.

Law, S.S., Li, X.Y. and Zhu, X.Q. (2005). "Structural damage detection from wavelet packet sensitivity", *Engineering Structures*, Vol. 27, No. 9, pp. 1339–1348.

Law, S.S. and Ding, Y. (2011). "Substructure methods for structural condition assessment", *Journal of Sound and Vibration*, Vol. 330, No. 15, pp. 3606–3619.

Lazarevic, A., Kanapady, R., Tamma, K., Kamath, C. and Kumar, V. (2003). "Damage prediction in structural mechanics using partitioning approach", *Proceedings of SPIE*, Vol. 5098, pp. 202–210.

Liu, C.C., Xu, J., Huang, J.H. and Yang, J. (2009). "Damage identification for transmission towers based on neural networks", *East China Electric Power*, Vol. 37, No. 2, pp. 256–260.

Lou, W.J. and Lin, B.L. (2006). "Wavelet transform based method for detecting damage location of electricity transmission towers", *Engineering Mechanics,* Vol. 23, No. 6, pp. 157–168.

Qu, W.L. and Peng, Q. (2007). "Damage detection method for vertical bars of mast structure in the time domain", *Journal of Earthquake Engineering and Engineering Vibration*, Vol. 6, No. 5, pp. 110–116.

Shi, Z.Y., Law, S.S. and Zhang, L.M. (1998). "Structural damage localization from modal strain energy change", *Journal of Sound and Vibration*, Vol. 218, No. 5, pp. 825–844.

Sun, Z.S., Ren, W.X. and Han, J.G. (2005). "Structural damage identification based on wavelet energy distribution vector", *Proceedings of the 9th International Conference on Inspection, Appraisal, Repairs and Maintenance of Structures*, Fuzhou, China, October, pp. 417–424.

Tan, D.M., Qu, W.L. and Qin, W.K. (2011). "Damage identification of transmission tower based on wavelet packet transform and fuzzy clustering", *Journal of Tianjin University*, Vol. 44, No. 8, pp. 695–700. (in Chinese)

Yan, W., Huang, T.L. and Ren, W.X. (2010). "Damage detection method based on element modal strain energy sensitivity", *Advances in Structural Engineering*, Vol. 13, No. 6, pp. 1075–1088.

Yen, G.G. and Lin, K.C. (2000). "Wavelet packet feature extraction for vibration monitoring", *IEEE Transaction Industrial Electronics*, Vol. 47, No. 3, pp. 650–667.

Yin, T., Lam, H.F., Chow, H.M. and Zhu, H.P. (2009). "Dynamic reduction-based structural damage detection of transmission tower utilizing ambient vibration data", *Engineering Structures*, Vol. 31, No. 9, pp. 2009–2019.

Zhu, H. (2009). "The neural network appraisal method of transmission tower structure damage by using time domain data", *International Conference on Energy and Environment Technology*, Guilin, China, October, pp. 344–347.

NOTATION

X_j^i	signal decomposition coefficients
E_j^i	signal energy at *i*th nodal floor at *j*th level resolution
$EC_{j,k}^i$	wavelet packet transform (WPT) energy curvature of the *i*th frequency band at the *k*th nodal
u	superscript stands for the original undamaged tower
d	superscript stands for the damaged tower
$E_{j,(k-1)}^i$	WPT energy at the (k–1)th nodal floor
$E_{j,k}^i$	WPT energy kth nodal floor
$E_{j,(k+1)}^i$	WPT energy (k+1)th nodal floor
$l_{(k-1),k}$	distance between the (k–1)th and kth nodal floor
$l_{k,(k+1)}$	distance between the kth and (k+1)th nodal floor
$l_{(k-1),(k+1)}$	distance between the (k–1)th and (k+1)th nodal floor
$ECCR_{j,k}^i$	change ratio of WPT energy curvature of the *i*th frequency band at the *k*th nodal floor
MSE_j^i	*i*th modal strain energy of the *j*th element
$\{\phi_i\}$	*i*th modal shape
$[K_j]$	element stiffness matrix of the *j*th element
$MSEC_j^i$	variation of modal strain energy
$MSECR_j^i$	modal strain energy change ratio
υ	mean value of normal distribution
σ	standard deviation of normal distribution
μ	upper limit of mean value with confidence probability $1 - \alpha$
$Index_j$	damage index of the *j*th member